NASA Technical Memorandum 104407

A Study of Three Dimensional Turbulent Boundary Layer Separation and Vortex Flow Control Using the Reduced Navier Stokes Equations

Bernhard H. Anderson
Lewis Research Center
Cleveland, Ohio

and

Saeed Farokhi
University of Kansas
Lawrence, Kansas

Prepared for the
Turbulent Shear Flow Symposium
Munich, Germany, September 9-11, 1991

NASA

A STUDY OF THREE DIMENSIONAL TURBULENT BOUNDARY LAYER SEPARATION AND VORTEX FLOW CONTROL USING THE REDUCED NAVIER STOKES EQUATIONS

by

Bernhard H. Anderson
NASA Lewis Research Center
Cleveland, OH 44135

and

Saeed Farokhi
University of Kansas
Lawrence, KS 66045

ABSTRACT

A Reduced Navier Stokes (RNS) initial value space marching solution technique has been applied to a class of vortex generator and separated flow problems and has demonstrated good predictions of the engine face flow field. This RNS solution technique using FLARE approximations can adequately describe the topological and topographical structure flow separation associated with vortex liftoff, and this conclusion led to the concept of a subclass of separations which can be called "vorticity separations", i.e. separations dominated by the transport of vorticity. Adequate near wall resolution of vorticity separations appears necessary for good predictions of these flows.

INTRODUCTION

This paper represents one in a series of studies on the design issues associated with inlet-engine compatibility problems, and in particular, engine face distortion and its control. These studies center on the development of CFD tools and techniques which look promising within an analysis-design environment, and the application of these new analysis approaches to understand and control inlet-engine distortion. The first paper in this series by Anderson (1991), deals with the aerodynamic characteristics of vortex interaction within the F/A-18 inlet duct, where the vortex interaction arises as a result of a vortex ingestion. Later studies will involve the effect of vortex ingestion on the engine face flow field itself. In the second paper in this series, by Anderson and Levy (1991), it was demonstrated that an installation of co-rotating vortex generators could be constructed to tailor the development of secondary flow to minimize engine face distortion. Of special interest is the conclusion that there exists an optimum axial location for this installation of co-rotating vortex generators, and within this configuration, there exists a maximum spacing between generators above which the engine face distortion increases rapidly. This study also showed that the vortex strength, generator scale, and secondary flow field structure have a complicated and interrelated influence on the engine face distortion, over and above the influence of the initial arrangement of generators.

Thus the overall goal of this paper is to advance the understanding and control of engine face distortion, and in particular, to effectively analyze the basic interactions that influence this important design problem. Specifically, the present paper achieves two goals: (1) it extends and validates a 3D RNS solution technique for class of vortex generator and separated flow problems which will be shown to be dominated by the transport of vorticity, and (2) it examines the role of near wall resolution for the class of vorticity dominated separated flow problems.

THEORETICAL BACKGROUND

The reduced Navier-Stokes (RNS) equations originally termed parabolized Navier-Stokes (PNS) equations and more recently semi-elliptic, or partially parabolic, are used here as an initial-value space marching method for the evaluation of subsonic compressible flow with strong interactions and/or separation arising from internal vortex flows. Techniques that use space marching with an approximate form of the RNS equations, namely initial-value methods and those that require three-dimensional global iterations, have been used for a number of years to predict flows in curved ducts and turbomachinery blade cascades. Unfortunately, this terminology does not identify the relevant mathematical approximations nor does it distinguish these approximations from the properties of the solution algorithm and the differential or difference equations. In other words, different methods within the same "category" will in some instances give significantly different results.

Three dimensional viscous subsonic flows in complex inlet duct geometries are investigated by a numerical procedure which allows solution by spatial forward marching integration, utilizing flow approximations from the velocity-decomposition approach of Briley and McDonald (1979 and 1984). The goal of this approach is to achieve a level of approximation that will yield accurate flow predictions, while reducing the labor below that needed to solve the full Navier Stokes equations. The governing equations for this approach have been given previously for orthogonal coordinates, and the approach has been applied successfully to problems whose geometries can be fitted conveniently with orthogonal coordinate systems. However, geometries encountered in typical subsonic inlet ducts cannot be treated easily using orthogonal coordinates, and this led to an extension of this approach by Levy, Briley, and McDonald (1983), to treat ducted geometries with nonorthogonal coordinates. The nonorthogonal capability has been validated over a wide range of inlet flow conditions.

Although the analysis itself was general, the class of ducted geometries that could be analyzed was represented by superelliptic cross-sections normal to a reference line space curve having continuous second derivatives. The description of the superelliptic cross-sections was specified by polynomials defined in terms of a marching parameter, τ. In generalizing the geometry formulation, Anderson (1991) extended the analysis to cover ducted geometries defined by an externally generated gridfile. This version of the 3D RNS computer code is called RNS3D. The geometry description within the gridfile is a "ducted" geometry which has a variable cross-sectional area and shape and a centerline which is curved and possibly twisted. In addition, the duct described by the gridfile is considered to have a defined centerline with continuous second derivatives. The surface geometry is described in terms of cross-sectional planes which lie perpendicular to the duct centerline, and thus represent the flow area at each streamwise station. Since the inlet duct geometry definition has been reduced to a cross section specification which is placed perpendicular to a centerline space curve, a number of grid and geometry pre-processing functions may be performed using RNS3D. These pre-processing functions include: (1) reclustering the existing gridfile mesh points for more accurate solutions in regions of high shear, (2) redefining the centerline space curve to satisfy design constraints, and (3) altering the cross-sectional shape of the inlet duct to reflect specified design iterations. The approach taken by Anderson (1991), is to develop a geometry pre-processor to augment the existing geometry and grid generation programs for internal inlet duct configurations, i.e. to partition the "work" of mesh generation between the grid generator and the flow solver.

RESULTS AND DISCUSSIONS

Comparison and Validation with Experimental Data

To demonstrate the accuracy of the numerical results obtained with RNS3D for internal duct flows typical of high angle-of-attack conditions, a series of numerical simulations were carried out using the University of Tennessee diffusing S-duct. In this experimental investigation sponsored by NASA Lewis Research Center Vakili, Wu, Liver, and Bhat (1986), obtained a series of measurements in a 30-30 degree diffusing S-duct of area ratio 1.5 with and without vortex generators (Fig. 1). The 30-30 degree circular cross-section S-duct, shown in Fig. 1, was made from two symmetric sections. The inlet duct diameter D_i was 16.51 cm. and the mean radius of curvature R was 82.55 cm. A straight pipe section of length $4.75D_i$ was installed upstream of the curved section to allow for the development of the turbulent boundary layer to the desired thickness. Another pipe of length $9.0D_e$ was installed downstream of the S-duct.

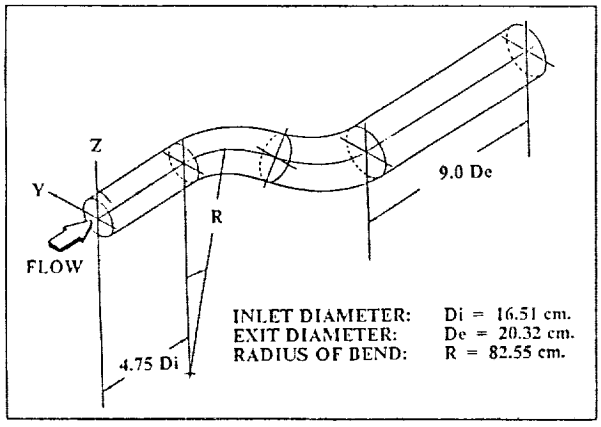

Fig. (1) Geometry definition of the Univ. Tennessee diffusing S-duct configuration.

All measurements were made at a nominal inlet Mach number of 0.60 at the reference measurement station in the straight section at $X/D_i = -1.54$. The flow parameters at this station were used as reference conditions for non-dimensionizing the experimental data. The experimental survey stations correspond to $X/D_i = 0.0$, 1.29, 2.49, and 5.2. At each survey station, a five-port cone probe was traversed radially at ten azimuthal angles, approximately 20 degrees apart, on both sides of the symmetry plane. At least seventy points were measured at each traverse.

A polar grid topology (Fig. 2), was chosen for the University of Tennessee diffusing S-duct, consisting of 49 radial, 49 circumferential, and 101 streamwise nodal points in the half-plane. The internal grid was constructed such that the transverse computational plane was perpendicular to the duct centerline. Grid clustering was used both in the radial and circumferential directions to redistribute the nodal points along these coordinate lines to resolve the high shear region near the wall and the separation region in the second bend. The flow in the inlet duct was turbulent, with an entrance Mach number of 0.6, Reynolds number based on an inlet diameter of 1.76×10^6, and the inflow corresponds to a shear layer $\delta/D_i = 0.05$. These initial conditions were applied at an axial station 1.54 inlet diameters (D_i) upstream of the duct entrance.

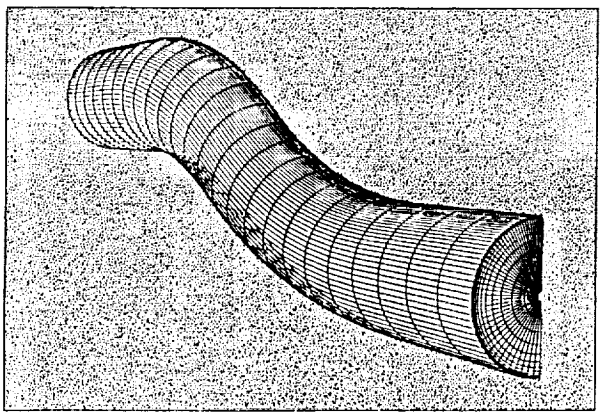

Fig. (2) Computation grid for the Univ. Tennessee diffusing S-duct configuration.

Fig. 3 shows a comparison between the experimental and computed total pressure coefficient contours at $X/D_i = 5.2$. In both the experiment and analysis, the flow in the S-duct separated and reattached in the second bend upstream of $X/D_i = 5.2$. This flow separation was caused by both adverse pressure gradients and the effect of pressure-driven secondary flow resulting from duct curvature. Experimental measurements and computational results from the 3D RNS code show excellent agreement for a simple mixing length turbulence model.

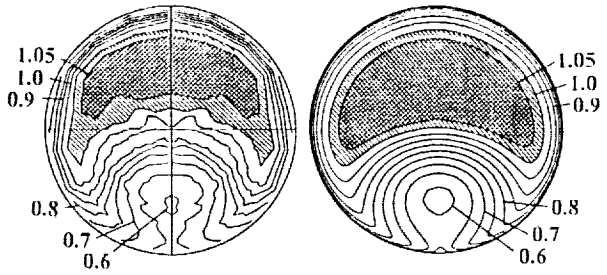

EXPERIMENTAL DATA ANALYSIS, y+ = 0.5

Fig. (3) Total pressure coefficient contours without vortex generators, $X/D_i = 5.2$.

As separation was encountered in the second bend of the S-duct, three pairs of vortex generator devices were installed in the duct at $X/D_i = 0.09$, and at azimuthal angles of -38.0, 0.0, and 38.0 degrees with respect to the streamwise direction. The vortex generator pairs had geometric incidence angles of +16.0 and -16.0 degrees relative to the duct centerline. Fig. 4 shows the comparison between the experimental and computed total pressure coefficient contours at $X/D_i = 5.2$. Comparison of contour levels between the separated case (Fig. 3), and the vortex generator case (Fig. 4), shows that the vortex generators successfully mixed the high energy core flow with the low energy flow in the wall region to suppress separation. In general, the computed interaction between the induced vortex generator flow and the pressure driven secondary flow was physically realistic and the agreement between experiment and analysis is considered very good, although more improvements on the generator model must be made.

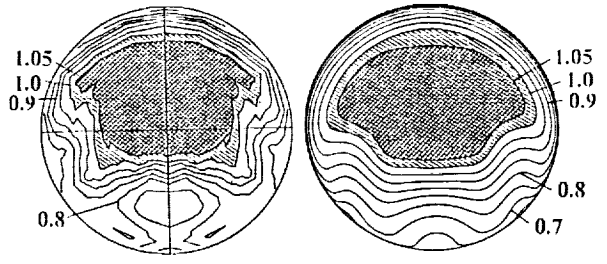

EXPERIMENTAL DATA ANALYSIS, y+ = 0.5

Fig. (4) Total pressure coefficient contours with vortex generators, $X/D_i = 5.2$.

Figs. 5 and 6 show additional flow characteristics obtained with the 3D RNS analysis with the vortex generator modeling. The secondary flow structure from the vortex generator model just downstream of the generator region, i.e. at $X/D_i = 0.18$, is shown in Fig. 5, and clearly reveals the three pairs of vortices that arise from the three pairs of counter-rotating generators. The limiting streamline signature shown

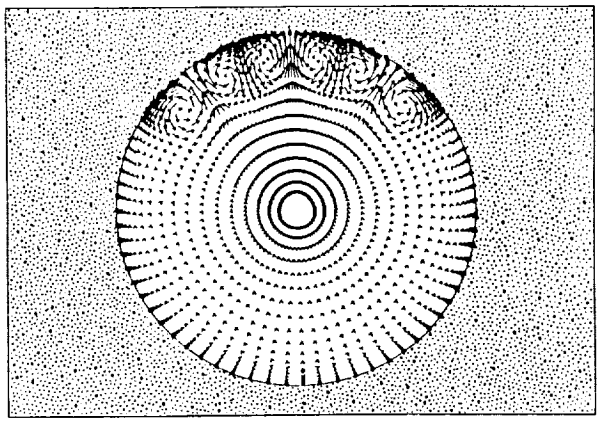

Fig. (5) Reduced Navier Stokes (RNS) solution showing secondary flow structure from vortex generator model, $X/D_i = 0.18$.

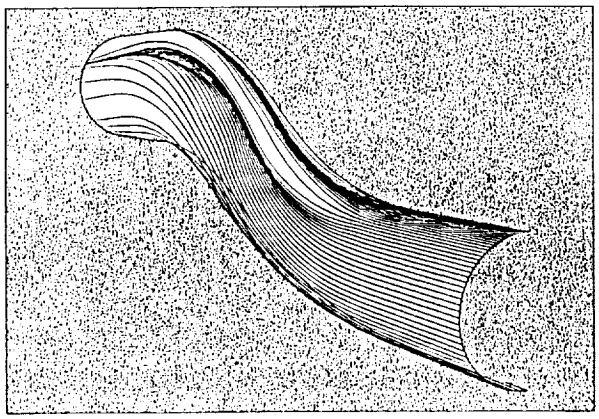

Fig. (6) Reduced Navier Stokes (RNS) solution showing limiting streamline signature of vortex generator region.

in Fig. 6 indicates that the generator configuration tested eliminated the flow separation encountered in the second bend, and reveals the familiar topographical pattern through the generator region itself.

Flow Separation and Vortex Liftoff

The three dimensional separation encountered in the University of Tennesse diffusing S-duct was very large in area and thin in extent (Figs. 7 and 8), and this separation did not alter the pressure distribution in a substantial manner. Secondary flow resulting from duct curvature caused an accumulation of boundary layer near the innerwall of the first 30 degree bend. The thick boundary layer thus established was

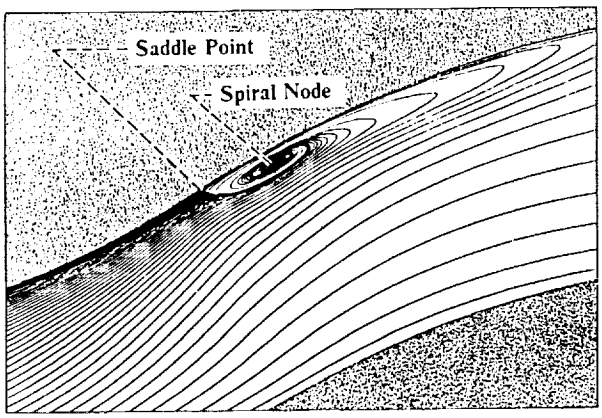

Fig. (7) Reduced Navier Stokes (RNS) solution showing limiting streamline signature of separation region within Univ. Tennessee diffusing S-duct.

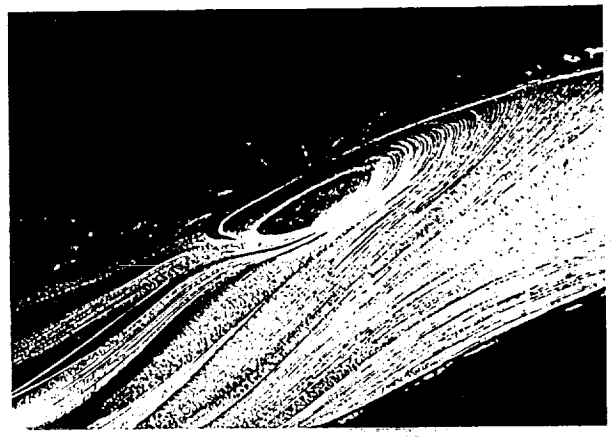

Fig. (8) Surface oil flow patterns showing separation region within Univ. Tennessee diffusing S-duct.

especially susceptible to flow separation because of the adverse pressure gradients induced by the reverse curvature section of the second 30 degree bend. A comparison between the computed oil flow patterns (represented by the limiting streamline topology in Fig. 7) and the experimental oil flow patterns presented in Fig. 8 shows excellent correspondence. Of exceptional importance is the fact that the space marching RNS analysis method using FLARE approximations captures the reverse flow region of this separation.

To meet the required confidence level of code validation, it is also essential that the 3D RNS marching analysis be able to capture the known topographical structure of the limiting streamlines in the vicinity of 3D separation. A very striking and significant feature captured by the analysis (Fig. 7), and seen in the oil flow pattern (Fig. 8), is the convergence of the limiting streamlines as an indication of three dimensional separation taking place in this duct. Another important and striking feature is the symmetric pair of spiral nodes and pair of saddle points that were clearly captured by the 3D RNS analysis. The topological patterns, as shown in the analysis Fig. 7, and the photograph of surface oil flow pattern Fig. 8, also reveal the remarkable characteristic that the limiting streamlines forming the spiral node enter only from downstream of the nodal point. The very familiar topological pattern shown in Figs. 7 and 8 is known to describe the important stage in the development of the pair of counter rotating vortices that form in the first 30 degrees of turning resulting in vortex liftoff in the second bend.

Table I presents a summary of the computed and experimental results for the separation characteristics in the University of Tennessee diffusing S-duct for RNS3D and two FNS (Full Navier Stokes) codes currently in use, PARC3D and CFL3D. In general, all three computer codes show remarkable consistancy with regard to the location of separation,

Source	Separation Point (X_s/D_i)	Reattachment Length ($\Delta X_r/D_i$)	Computational Grid ($N_\theta \times N_R \times N_x$)	CPU Time (Min.)
RNS (RNS3D)	2.5	2.6	49x49x95	6.5
FNS (PARC3D)	2.4	1.7	26x49x65	600.0+
FNS (CFL3D)	2.4	2.6	26x49x65	600.0+
Experiment	1.8	1.2	———	———

Table I Summary of computed and experimental separation characteristics for the Univ. Tennessee diffusing S-duct.

while two codes, RNS3D and CFL3D, show very good agreement with regard to the reattachment length. However, none of the computer codes showed very good agreement with regards to this particular set of experimental data. In general, RNS3D was able to capture the essential features of separation location and reattachment length as well as the two PNS solutions, certainly with far more computational efficiency.

The topography of this very important flow interaction is shown schematically in Fig. 9, while Figs. 10 and 11 show the computed particle traces associated with vortex liftoff for particles orignating at $y/\delta_i = 0.03$ (Fig. 10), $y/\delta_i = 0.30$ (Fig. 11).

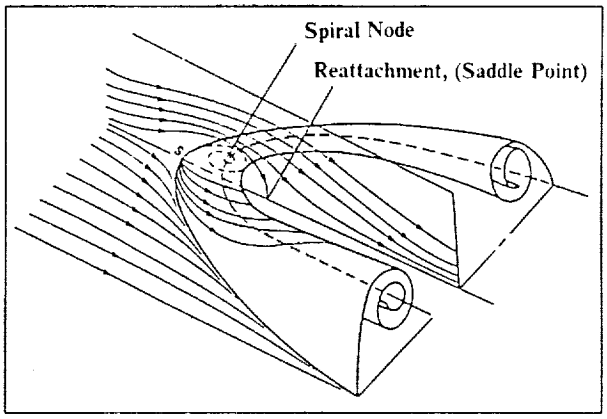

Fig. (9) Topography of the streamlines associated with vortex liftoff.

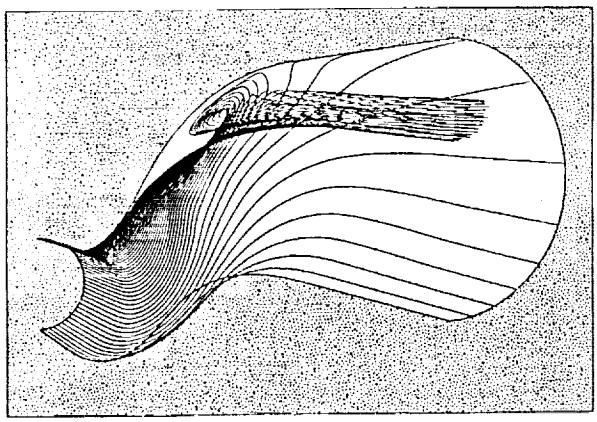

Fig. (10) Reduced Navier Stokes (RNS) solution showing particle traces associated with vortex liftoff, $y^+ = 0.5, y/\delta_i = 0.03$.

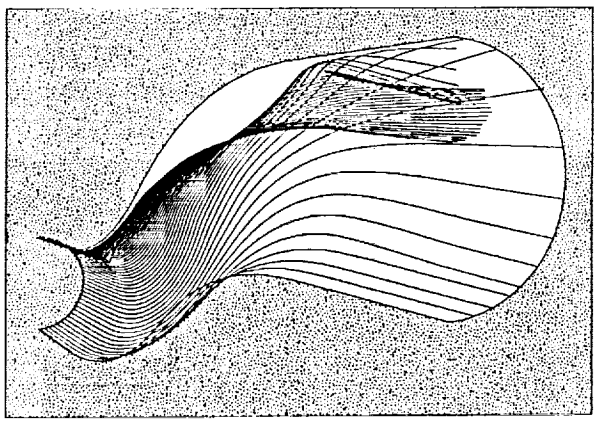

Fig. (11) Reduced Navier Stokes (RNS) solution showing particle traces associated with vortex liftoff, $y^+ = 0.5, y/\delta_i = 0.30$.

It is quite apparent that fluid particles that originate well inside the entrance boundary layer can influence the core region of the engine face station.

In general, the flow separation studied here was dominated by pressure forces rather than shear forces, as would be the case with massive separation in the inlet duct, such that the influence of the stress-driven flows was small and the effective viscosity approach surprisingly successful. In order to explain the success of space marching 3D RNS methods in describing the detailed topographical structure of vortex liftoff, it must be concluded that there exists a class of separated flows that are dominated by the transport of vorticity. This class of separation interactions can be called "vorticity separations", since they differ fundamentally from shear-driven separations.

Vorticity Dominated Internal Flow Fields

Several numerical factors can affect the accuracy of predictions of high Reynolds number vorticity-dominated internal flows. These include (1) the nature of numerical smoothing (in the case of Full Navier Stokes analyses), (2) the kind of turbulence model used to describe the turbulent transport properties, and (3) the form of the grid distribution to resolve the details of the viscous boundary layer in the near wall region where the vorticity is the largest. For the computations of the flow within the University of Tennessee diffusing S-duct, two calculations were made to study the effects of near wall grid resolution. In the first case, the radial grid spacing was chosen to give a nominal y^+ of 8.5 at first grid point above the duct wall, and in the second case, a nominal y^+ value of 0.5 was chosen, both determined at the duct enterence plane $X/D_i = 0.0$. Figs. 12 and 13 show the effects of this near wall grid lattice resolution on the total pressure coefficient contours (Fig. 12), and the secondary flow structure (Fig. 13), both at the engine face station, $X/D_i = 5.2$. It was the case of $y^+ = 0.5$ which gave the best agreement with the experimentally measured engine face flow field (see Fig. 3). The very strong effect of near wall grid resolution on structure and strength of the engine face flow results from the very nature of vorticity dominated internal flows. Since the largest value of vorticity occurs in the near wall region, and secondary flow is generated by turning of transverse shear, a very strong effect of near wall grid resolution was realized as stronger secondary flow (Fig. 13), which had consequently an appreciable influence on the primary flow (Fig. 12). This interaction is really an inviscid

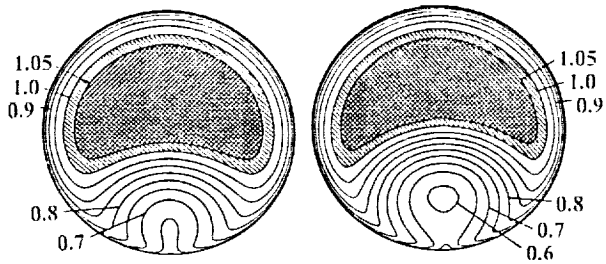

Fig. (12) Effect of near wall grid lattice resolution on total pressure coefficient contours, $X/D_i = 5.2$.

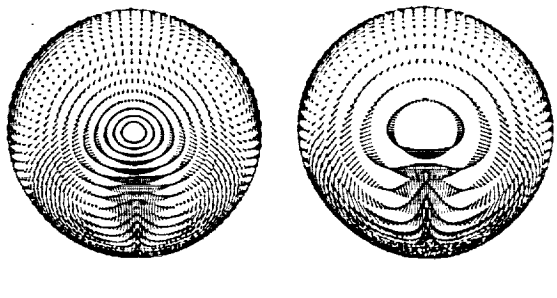

Fig. (13) Effect of near wall grid lattice resolution on secondary flow structure, $X/D_i = 5.2$.

rotational phenomenon rather than a viscous phenomenon, and indicates that secondary flow has its ultimate origin very near the wall. The turbulence model will thus also strongly influence the strength of secondary flow, but only as an invsicid rotational phenomena through the near wall vorticity distribution and not necessarily as part of the turbulent properties of the flow.

Figs. 14 and 15 show the limiting streamline signatures obtained with the Reduced Navier Stokes code for $y^+ = 8.5$ (Fig. 14) and for $y^+ = 0.5$ (Fig. 15). Both figures clearly reveal the size of the flow separation region encountered in the University of Tennessee diffusing S-duct, as well as the characteristic topology associated with vortex liftoff. However, there is a marked difference in the calculated extent of the separated region between the two cases, i.e. lack of near wall resolution diminishes the size of the separated region. It is quite evident that near wall resolution plays a very important role in determining the structure of the separation associated with vortex liftoff.

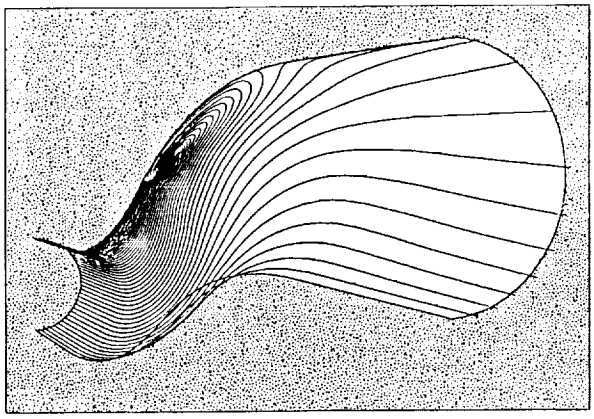

Fig. (14) Reduced Navier Stokes (RNS) solution showing limiting streamline signature of separation region, $y^+ = 8.5$.

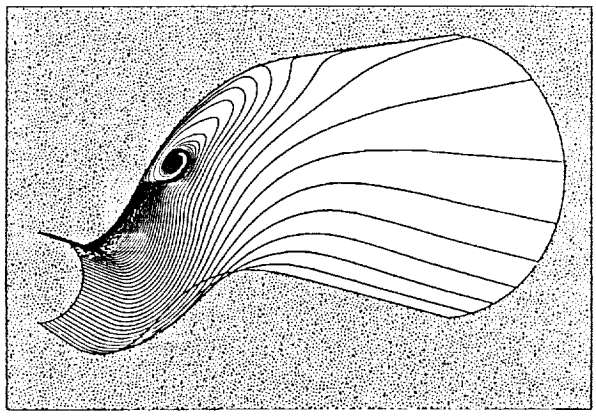

Fig. (15) Reduced Navier Stokes (RNS) solution showing limiting streamline signature of separation region, $y^+ = 0.5$.

The significance of near wall resolution with regards to engine face distortion is presented in Figs. 16 and 17, where the distortion parameters used for comparision are the more advanced ring distortion descriptors, introduced in the late 1960's and 1970's. These parameters, which are defined by Anderson (1991), take into account the distortion of each ring of total pressure measurements, or in this case, at each ring of the radial computational mesh. In comparing the two calculations in Figs. 16 and 17, it can be seen that a maximum difference of 0.02 can be incurred in the radial pressure ring distortion, while a maximum uncertainty of 0.01 can be realized in the calculation of the 60°-sector circumferential ring

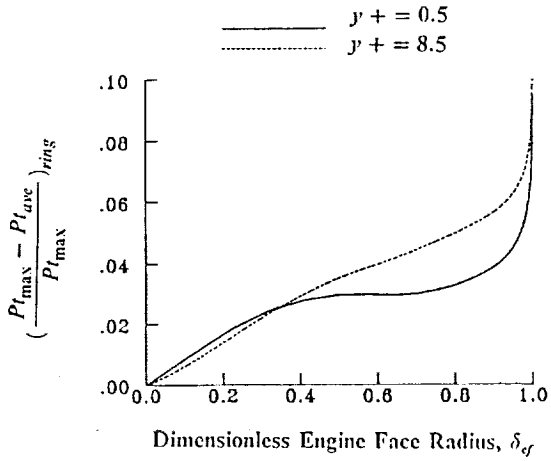

Fig. (16) Effect of near wall resolution (y^+) on engine face radial pressure ring distortion.

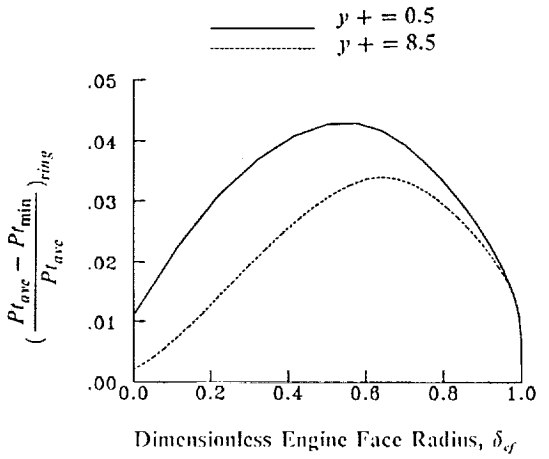

Fig. (17) Effect of near wall resolution (y^+) on engine face 60°-sector circumferential pressure ring distortion.

distortion descriptor. The uncertainty of 0.01 represents a 33% error in the maximum 60°-sector circumferential ring distortion indicator.

CONCLUSIONS

The present results provide a validation of the initial value space-marching 3D RNS procedure and demonstrates accurate predictions of the compressor face flow field, with a separation present in the inlet duct as well as when vortex generators are installed to suppress separation. The computing time, CPU = 6.5 min. on the CRAY XMP for 2.28×10^5 grid points, for both the baseline case and the case with three pairs of counter-rotating vortex generators, is sufficiently rapid for routine use in an analysis-design engineering environment.

Initial value space marching 3D RNS procedures using FLARE approximations can adequately describe the topological and topographical features of 3D flow separations associated with vortex liftoff within inlet ducts. The success of this RNS analysis in describing this phenomenon is due to the existence of a class of separated flows, which can be called "vorticity separations", which are dominated by the transport of vorticity rather than turbulent shear effects.

Adequate near wall resolution of "vorticity separated" turbulent flows are necessary to obtain accurate calculations of the strength of secondary flows that develop in typical inlet ducts, and in particular, the size and shape of the separated region and the engine face total pressure recovery map and distortion level.

REFERENCES

ANDERSON, BERNHARD H. 1991 The Aerodynamic Characteristics of Vortex Ingestion for the F/A-18 Inlet Duct. AIAA Paper No. 91-0130.

ANDERSON, BERNHARD H. & LEVY, RALPH 1991 A Design Strategy for the Use of Vortex Generators to Manage Inlet-Engine Distortion Using Computatinal Fluid Dynamics. AIAA Paper No. 91-2474.

BRILEY, W. R., & MC DONALD, H. 1979 Analysis and Computation of Viscous Subsonic Primary and Secondary Flow. AIAA Paper No. 79-1453.

BRILEY, W. R., & MC DONALD, H. 1984 Three-Dimensional Viscous Flows with Large Secondary Velocities. Journal of Fluid Mechanics, 144, 47-77.

LEVY, R., BRILEY, W. R., & MC DONALD, H. 1983 Viscous Primary/Secondary Flow Analysis for Use with Nonorthogonal Coordinate Systems. AIAA Paper No. 83-0556.

VAKILI, A. D., WU, J. M., LIVER, P. A., & BHAT, M. K. 1986 Experimental Investigation of Secondary Flows in a Diffusing S-Duct with Vortex Generators. NASA NAG-233.

NASA
National Aeronautics and Space Administration

Report Documentation Page

1. Report No.	2. Government Accession No.	3. Recipient's Catalog No.
NASA TM -104407		

4. Title and Subtitle
A Study of Three Dimensional Turbulent Boundary Layer Separation and Vortex Flow Control Using the Reduced Navier Stokes Equations

5. Report Date

6. Performing Organization Code

7. Author(s)
Bernhard H. Anderson and Saeed Farokhi

8. Performing Organization Report No.
E -6233

10. Work Unit No.
505 -62-52

9. Performing Organization Name and Address
National Aeronautics and Space Administration
Lewis Research Center
Cleveland, Ohio 44135 - 3191

11. Contract or Grant No.

13. Type of Report and Period Covered
Technical Memorandum

12. Sponsoring Agency Name and Address
National Aeronautics and Space Administration
Washington, D.C. 20546 - 0001

14. Sponsoring Agency Code

15. Supplementary Notes
Prepared for the Turbulent Shear Flow Symposium, Munich, Germany, September 9-11, 1991. Bernhard H. Anderson, NASA Lewis Research Center; Saeed Farokhi, University of Kansas, Lawrence, Kansas 66045. Responsible person, Bernhard H. Anderson, (216) 433-5822.

16. Abstract
A Reduced Navier Stokes (RNS) initial value space marching solution technique has been applied to the class of vortex generator and separated flow problems and has demonstrated good predictions of the engine face flow field. This RNS solution technique using FLARE approximations can adequately describe the topological and topographical structure flow separation associated with vortex liftoff, and this conclusion led to the concept of a subclass of separations which can be called "vorticity separations", i.e. separations dominated by the transport of vorticity. Adequate near wall resolution of vorticity separations appears necessary for good predictions of these flows.

17. Key Words (Suggested by Author(s))
Computational fluid dynamics
Applied aerodynamics
Internal flow

18. Distribution Statement
Unclassified - Unlimited
Subject Category 02

19. Security Classif. (of the report)	20. Security Classif. (of this page)	21. No. of pages	22. Price*
Unclassified	Unclassified	8	A02

NASA FORM 1626 OCT 86

*For sale by the National Technical Information Service, Springfield, Virginia 22161